Performance Assessment of Dual-Polarized 5G Waveforms and Beyond in Directly Modulated DFB-Laser using Volterra Equalizer

O.Gharbi,[a]* S.Mhatli,[a] , I.Dayoub,[b] S.Haxha,[c] R. Attia,[a] Adel Aldalbahi,[d] and M.Jassim[e]

[a] SERCOM Laboratory, Tunisia Polytechnic School, Carthage University, Tunis 2078, Tunisia.

[b] Université Polytechnique Hauts-de-France, CNRS, University Lille, ISEN, Centrale Lille, UMR 8520 IEMN, DOAE, Le Mont Houy, Valenciennes, France.

[c] Departement of Electronic Engineering Microwave Photonics and Sensors, University of London, UK.

[d] King Faisal University, Hofuf 31982, Saudi Arabia

[e] Department of electrical and computer engineering, Valpariso University, Valpariso, IN, USA Department of Electrical and Computer Engineering, Valparaiso University, Valparaiso, IN, USA

Abstract: In this paper, we investigate the performance of 25 Gbps dual-polarized OFDM-based modulation in directly modulated DFB-laser over 25 Km of single-mode fiber. Volterra equalizer is used to compensate the nonlinear effects of the optical fiber. The results show that FBMC-OQAM modulation outperforms OFDM, UFMC and GFDM waveforms. Indeed, a target of BER ~ 3.810^{-3} (FEC limit) for FBMC, UFMC, OFDM and GFDM can be achieved at -30.5,-26, -16 and -14.9 dBm, respectively. The effect of DFB laser is also investigated for UFMC, OFDM and GFDM, they undergo a *Q* penalty of 2.44, 2.77 and 4.14 dB, respectively, at their FEC limit points. For FBMC-OQAM, the signal is perfectly recovered when excluding the DFB laser at -30.5 dBm.

Keywords: 5G networks and Beyond, DFB Laser, FBMC, GFDM, OFDM, UFMC, Volterra Equalizer.

* First Author**,** E-mail: oussama_gharbi@yahoo.com

1. Introduction

In fifth-generation networks, three main use cases are stipulated by the International Mobile Telecommunications (IMT) vision recommendations [1] namely, enhanced Mobile Broadband (eMBB), Ultra-Reliable Low Latency Communications (URLLC) and massive Machine Type Communications (mMTC).

For the eMBB scenario, it requires a wide coverage area and high data rate to support the emerging multimedia services such as Ultra-High Definition (U-HD) resolution and holographic type communication such as Augmented Reality and Virtual Reality (AR/VR) gaming which is considered as a pillar for beyond 5G vision [2]. Indeed, videos will represent 75% of data traffic by 2022 [3]. For URLLC, it is characterized by a stringent requirement on latency and reliability for critical communications, e.g. Remote surgery, Vehicle-to-everything (V2X). Accordingly, the upcoming 6G networks consider a very low latency in both fronthaul and backhaul in order to meet the high demands of data traffic [4]. Finally, mMTC, known also as Internet of things (IoT), aims to connect a massive number of devices with low power consumption.

To accommodate these various scenarios, a new flexible air interface [5] and innovative scheme of the radio access network, known as Centralized Radio Access Network (C-RAN), are introduced.

The 4G air interface is based on Orthogonal Frequency Division Multiplexing (OFDM) due its high spectral efficiency when compared with Frequency Division Multiplexing (FDM) by overlapping orthogonal subcarriers, its robustness against multipath fading (narrowband subcarriers, cyclic prefix) and its low complexity where the modulation is performed by Inverse Fast Fourier Transform (IFFT) [6]. However, OFDM system suffers from a high Peak to

Average Power Ratio (PAPR), which requires a high linearity of amplifiers. It has a large Out-of-Band (OOB) radiation caused by the square pulse shaping filter. Also, the use of Cyclic Prefix (CP) in each OFDM symbol decreases both data rate and spectral efficiency of the signal and poses a challenge for the low latency use case. Furthermore, with OFDM, it is challenging to support applications in massive connection due to the strict synchronization.
To overcome these limitations, several waveforms based on OFDM modulation are proposed for 5G and beyond air interface technology, such as Filter Bank Multicarrier (FBMC) [7], Universal Filtered Multicarrier (UFMC) [8] and Generalized Frequency Division Multiplexing (GFDM) [9]. On the other hand, the basic idea behind C-RAN technology is to aggregate the Base Band Units (BBUs) at the central location known as BBU hotel which is placed away from the Remote Radio Head (RRH) as shown in Fig.1.
The principal advantages of C-RAN are:
Cost-effective: to meet the eMBB constraints, many cell towers need to be deployed, which makes the management operation more complicated. Furthermore, in the traditional radio access network, each BBU and RRH requires its cooling system. Fortunately, with the emerging of C-RAN configuration, the base station installation is simplified and the air-conditioner system can be abandoned at the antenna site, which can reduce the operational expenditures (OPEX) and capital expenditures (CAPEX) [10]. To give an idea, six sites based on C-RAN technology can reduce the equipment costs by 9%, 30% of construction costs and around 76% of operation and maintenance tasks. [11].
Low latency: URLLC scenario can be achieved with C-RAN technology. Indeed, the BBUs aggregation at the same location reduces the time of information exchange between them [12]. The two components of C-RAN architecture (i.e. BBUs and RRHs) are connected utilizing Fronthaul and Backhaul segments based on the optical link.

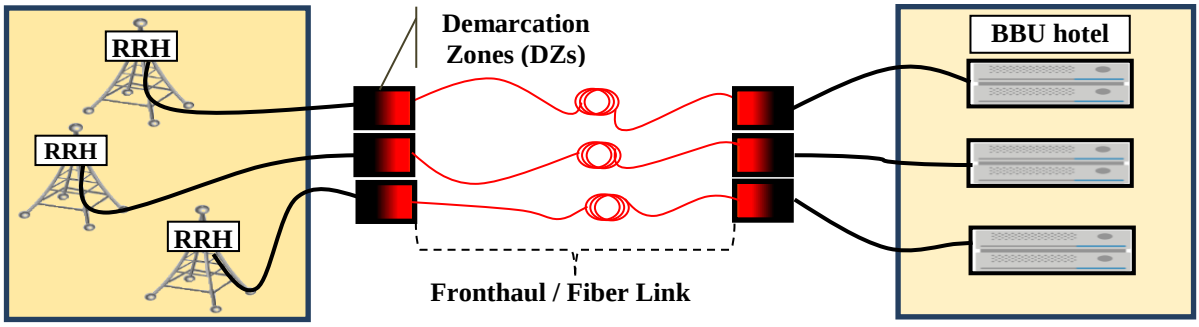

Fig.1 Centralized RAN scheme with Fronthaul segment [13]

In optical communications, OFDM has been extensively addressed [14] either in coherent detection or in Intensity Modulation Direct Detection (IM-DD) systems. In literature, much work on the potential of optical OFDM-based for 5G networks and beyond has been carried out, but most of them have considered either Mach-Zehnder interferometer [15] or ideal intensity modulator [16]. But, some areas still uninvestigated, in particular, the cost-effective, compact size and low power consumption of the Distributed FeedBack laser (DFB) [17].
Our objective here is to contribute to low-cost and lower-power consumption 5G networks and beyond based on C-RAN architecture.
Though, in Directly Modulated Lasers (DMLs), the output signal is commonly accompanied by a series of relaxation oscillations generated by the abrupt change of the current density [18]. This chirp leads to a spectral broadening of the signal and when coupled with the fiber dispersion, the intermixing interferences among subcarriers occur and degrade the system performance.
To face these non-linear effects, we propose an electrical compensation technique based on Volterra series [19].

For the first time, we investigate the performance of the dual-polarized 16-QAM OFDM-based modulation in directly modulated DFB-laser based on IM-DD architecture using the Volterra equalizer.
The rest of this paper is organized as follows: Section 2 gives a brief overview of the proposed 5G waveforms and beyond. Section 3 describes the transmission model link. Simulation results are discussed in section 4. Section 5 focuses on waveforms computational complexity and finally, some conclusions are drawn in Section 6.

2. 5G Waveforms and Beyond

The OFDM waveform adopts a rectangular pulse shape for the analysis and synthesis filters even for practical cases where the channel is not flat. It is translated into bad frequency localization (i.e. poor energy concentration) with high OOB emission, which poses a big challenge for asynchronous communications. Hence some modifications need to be introduced in the filtering stage to improve these weaknesses and design new waveforms. In this section, we briefly describe the FBMC, UFMC and GFDM modulations.

2.1. Filter Bank Multicarrier (FBMC)

Filter Bank Multicarrier (FBMC), proposed for the first time by Saltezbeg [20], is an evolution of OFDM. The main idea is to substitute the rectangular pulse shaping filter with a well-designed filter with good time-frequency localization and low spectral leakage. The filtering process is applied per subcarrier. The PHYDYAS filter [21] is widely used in the literature and its realization is based on the frequency sampling technique [22], which consists of determining the frequency coefficients that comply with the Nyquist criteria and build from these coefficients the frequency response by interpolation. The impulse response is given by applying IFFT. The determination of the frequency coefficients depends on the overlapping factor $K = L/M$, where L is the number of coefficients of the impulse response of the filter and M is the number of subcarriers.
The frequency response of PHYDYAS filter with M subcarrier is given by [23]:

$$C(f) = \sum_{k=-(K-1)}^{K-1} C_k \frac{\sin(\pi(f - \frac{k}{MK})MK)}{MK \sin(\pi(f - \frac{k}{MK})} \qquad (1)$$

where C_k is the frequency coefficients of the filter. For K=4, the frequency domain coefficients are:

$$C_0=1, \quad C_{\pm1}=0.97196, \quad C_{\pm2}=\frac{\sqrt{2}}{2}, \quad C_{\pm3}=0.235147$$

For long filter length (i.e. increase K), FBMC becomes more robust against multipath fading (i.e. fiber dispersion in optical communication). Thus, the cyclic prefix can be discarded.
Unlike OFDM, the orthogonality must be ensured only for neighboring subcarriers and to fulfill this constraint, Offset-QAM (O-QAM) is used, where the orthogonality is achieved only in the real domain (i.e. real or imaginary part), this modulation scheme is known as FBMC-OQAM. In addition, the output signals after the O-QAM process is either real or imaginary valued [24]. In [23], the authors have proposed a low complexity implementation for FBMC by combining a PolyPhase Network (PPN) with IFFT/FFT, wherein the filter coefficient of length $L=K\times M$ can be decomposed into M interleaved sequence of K coefficients. FBMC is an attractive modulation scheme for cognitive radio systems compared to the conventional OFDM due to its high spectral efficiency [25]. Moreover, one of the interesting finding in [26], is the

coexistence between five intra-bands carrier-aggregated based on FBMC signals and three intra-bands carrier-aggregated LTE-A signals with high capacity. Fig.2 illustrates the block diagram of the transmission system.

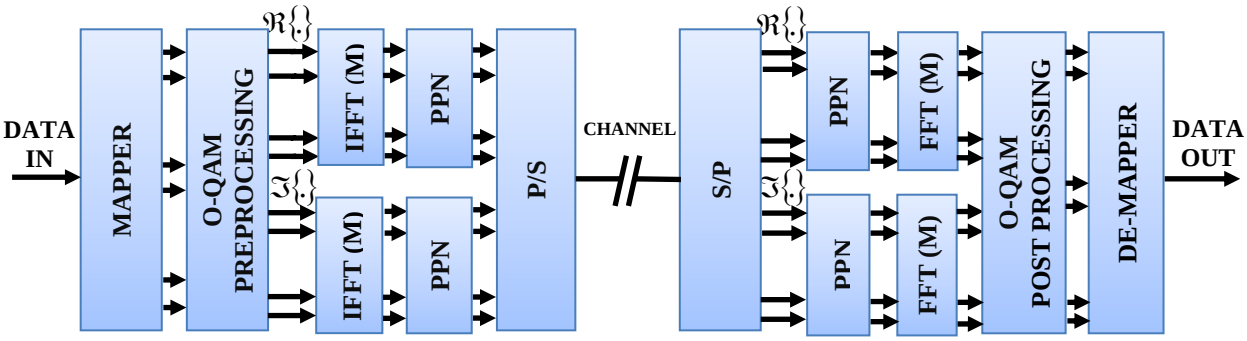

Fig.2 Block diagram of FBMC-OQAM with PPN transceiver

2.2. Universal Filtered Multicarrier (UFMC)

The system structure for UFMC is shown in Fig. 3. In this technique, the total available bandwidth is split into several sub-bands. Each sub-band is filtered by the Dolph-Chebyshev window of length *L*, which is typically equal to the cyclic length of the traditional OFDM. Hence, the UFMC adopted a short filter duration compared to FBMC (i.e. a multiple of overlapping factor *K*) and considered as the best choice for IoT communications with short bursts transmission [27].

Because of the linear convolution between *M*-point IFFT and Finite Impulse Response (FIR) filter with length *L*, the UFMC symbol has the length of M + L - 1. Thus, zeros are padded to apply 2*M*-point FFT. The magnitude of the frequency response function for the Dolph-Chebyshev can be expressed as [28]:

$$|H(j\omega)| = \frac{1}{\sqrt{1+\varepsilon^2 C_N{}^2(\frac{\omega}{\omega_c})}} \qquad (2)$$

In (2), ε is a parameter that controls the amplitude of the oscillations, ω_c is the 3db cut-off frequency and C_N is the *Nth* order of Chebyshev polynomial.

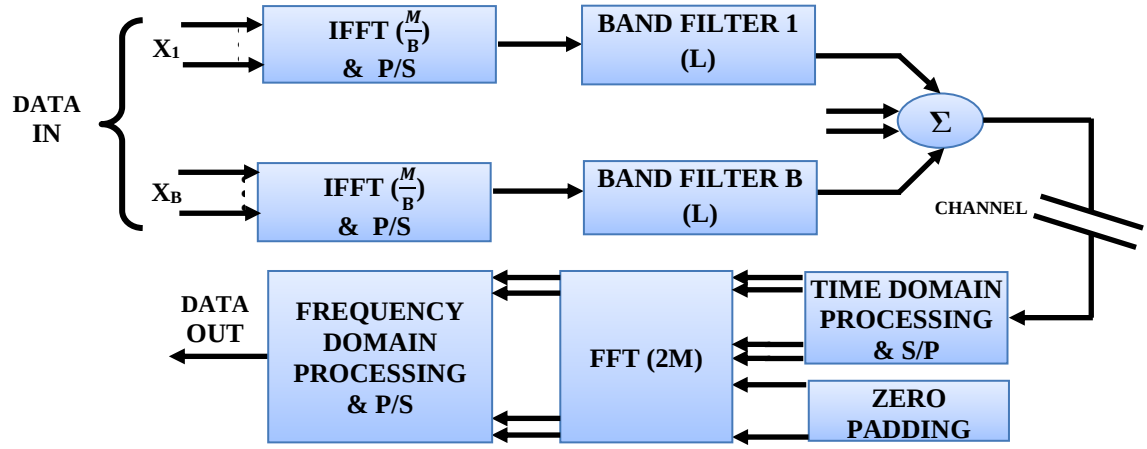

Fig.3 Block diagram of UFMC transceiver [27]

2.3. Generalized Frequency Division Multiplexing (GFDM)

Generalized Frequency Division Multiplexing was primarily suggested by G. Fettweis et al. [9]. In GFDM, a block of $M \times T$ symbols is transmitted over M subcarriers and T timeslots. Unlike FBMC and UFMC as well, GFDM uses circular convolution between data symbols and the transmit filter by mean of a technique called tail-biting to circumvent the filter spreading [29]. In other words, the CP length is reduced, leading to high spectral efficiency. Also, CP is appended after T timeslots rather than a CP per symbol in OFDM (i.e. one timeslot). To deal with different scenarios, GFDM shows high flexibility. For example, the low latency requirement can be fulfilled by reducing the number of timeslots T and for T=1, the traditional OFDM is obtained. In this case, the number of subcarriers M must be increased, leading to high spectral bandwidth. Also, for narrow bandwidth signal and low PAPR, we can decrease the number of subcarriers M at the cost of raising the latency. Some trade-offs between frequency resource allocation and latency have to be made.

GFDM is considered as a non-orthogonal waveform, where the Raised Cosine (RC) or Root Raised Cosine (RRC) filters are used with a roll-off factor α, ranged from 0 to 1 which describes how much the adjacent subcarriers overlap in the frequency domain.

The frequency response of the RRC filter can be given as [30]:

$$G_{RRC}(f) = \sqrt{\frac{1-\cos(\pi \times lin_{\alpha}(\frac{f}{T}))}{2}} \qquad (3)$$

where T is the number of timeslots. The truncated linear function $\text{lin}_{\alpha}(\frac{f}{T})$ can be used to characterize the roll-off area in the frequency domain and defined as:

$$lin_{\alpha}(\frac{f}{T}) = \min\left(1, \max\left(0, \frac{1+\alpha}{2\alpha} + \frac{|\frac{f}{T}|}{\alpha}\right)\right) \qquad (4)$$

Some techniques are used to recover the orthogonality between subcarriers caused by the prototype filter, namely, Serial Interference Cancellation (SIC) and double side SIC [31].

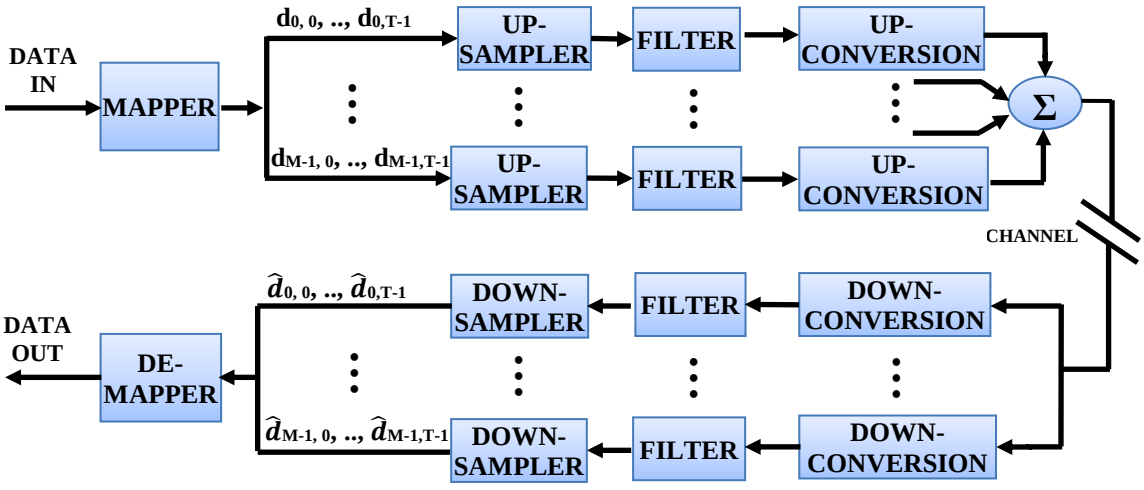

Fig.4 Block diagram of GFDM transceiver [32]

3. Simulation Setup

All the simulations and results are developed and obtained using MATLAB program.

As sketched in Fig.5, we employed the Two-Input Two-Output (TITO) model [14] to double the channel capacity of the system.

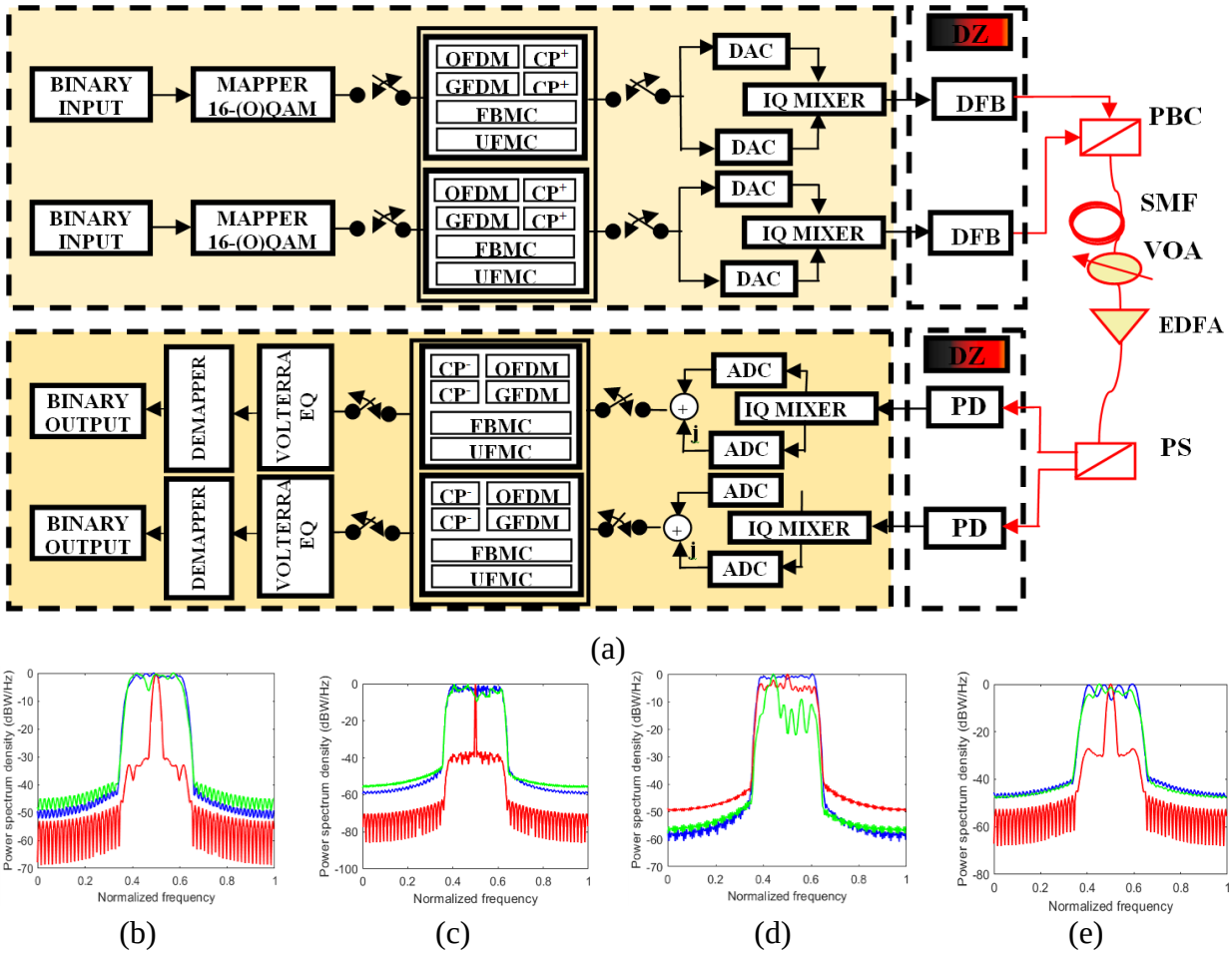

Fig. 5 (a) Block diagram of the system. (b) OFDM spectrum for the emitted signal (*blue*), received signal before Volterra (*red*) received signal after Volterra (*green*). GFDM, FBMC and UFMC spectrum are shown in (c), (d) and (e), respectively. CP: Cyclic Prefix, DAC: Digital to Analog Converter, PBC: Polarization Beam Combiner, SMF: Single-Mode Fiber, VOA: Variable Optical Attenuator, EDFA: Erbium-Doped Fiber Amplifier, PS: Polarization Splitter, PD: Photo-Detector, ADC: Analog to Digital Converter.

The evolution of the two optical vectors, A_x and A_y, are modeled by Manakov equations which can be defined as [33]:

$$\frac{\partial A_x}{\partial z} - j\frac{\beta_2}{2}\frac{\partial^2 A_x}{\partial t^2} + \frac{\alpha}{2}A_x = -j\frac{8}{9}\gamma(|A_x|^2 + |A_y|^2)A_x \qquad (5)$$

$$\frac{\partial A_y}{\partial z} - j\frac{\beta_2}{2}\frac{\partial^2 A_y}{\partial t^2} + \frac{\alpha}{2}A_y = -j\frac{8}{9}\gamma(|A_y|^2 + |A_x|^2)A_y \qquad (6)$$

where β_2 the Group Velocity Dispersion (GVD) parameter, α is the fiber loss coefficient , γ is the Kerr nonlinear coefficient , z and t are spatial and temporal variables, respectively. In order to numerically solve Eq.(9) and (10), the Asymmetric Split-Step Fourier Method (A-SSFM) is used. In this technique, the entire fiber length is divided into several sections of length h. For each section, the linear effects are computed in frequency domain over the first half (i.e.

h/2) and the nonlinear contributions are evaluated in time domain over the second half of the segment.

In this section, a data rate of 25Gbps (i.e.2x12.5Gbps) signals are generated using the parameters summarized in Table I and II.

Table I. System simulation parameters

Waveform Parameter	**Value**
OFDM	
IFFT/FFT size	64/64
Modulation	16-QAM
Cyclic prefix length (%)	12.5
Prototype filter	Rectangular
Data rate (Gbps)	12.5
FBMC	
IFFT/FFT size	64/64
Modulation	16-OQAM
Prototype filter	PHYDYAS
Overlapping factor	4
Data rate (Gbps)	12.5
UFMC	
IFFT/FFT size	64/128
Sub-band Size	16
# of Sub-bands	4
Modulation	16-QAM
Prototype filter	Dolph-Chebyshev
Filter length	9
Sidelobe attenuation (dB)	40
Data rate (Gbps)	12.5
GFDM	
IFFT/FFT size	64/64
Active Subcarriers / #of timeslots	32/7
Modulation	16-QAM
Cyclic prefix length (%)	12.5
Prototype filter	RRC (α= 0.1)
Data rate (Gbps)	12.5

Table II. Optical link parameters

Optical component	**Value**
DFB laser	
Bias current (mA)	35
Peak-to-peak current (mA)	15
Wavelength (nm)	1550
Single-mode fiber	
Chromatic dispersion (ps/km.nm)	17
Group velocity dispersion (s^2/m)	-21.7×10^{-27}
PMD coefficient (ps/$\sqrt{\text{km}}$)	0.1
Attenuation (dB/Km)	0.2
Kerr coefficient (km^{-1} W^{-})	1.3
Span length (Km)	25
SMF core area (m^2)	80×10^{-12}
PotoDiode (APD)	
Responsivity (A/W)	0.9
APD gain	20
Bandwidth (GHZ)	80
EDFA amplifier	

Noise figure (dB)	5.5
Gain (dB)	20

It is worth noting that for FBMC, the overlapping factor *K* of PHYDYAS filter is set at its optimum value, 4 [34] and for GFDM modulation, only 32 subcarriers among 64 are used to carry out data in order to minimize the effects of the interference between subcarriers caused by the loss of orthogonality and the roll-off factor of 0.1 is considered to reduce the overlapping between adjacent filters.

One of the main challenges for the optical IM-DD system is the rising of nonlinear effects generated by the interaction between laser chirp and fiber dispersion (i.e. Group Velocity Dispersion), which exhibit subcarrier-to-subcarrier intermixing interferences (SSII) after law square detection. SSII mitigation can be achieved by nonlinear filtering. Volterra-based nonlinear equalization is an attractive tool to compensate these impairments [35], [36].

The Volterra series expansion can be assimilated to a Taylor series with memory where the current output relies on previous inputs. The discrete-time input-output relation of full Volterra series can be defined as [37]:

$$\begin{aligned} \mathrm{Y(n)}= h_0 + \sum_{i_1=0}^{\infty} h_1(i_1)x(n-i_1) + \sum_{i_1=0}^{\infty}\sum_{i_2=0}^{\infty} h_2(i_1,i_2)x(n-i_1)x(n-i_2) \\ + \cdots \sum_{i_1=0}^{\infty}\cdots\sum_{i_j=0}^{\infty} h_j(i_1 \ldots i_j)x(n-i_1)\ldots x(n-i_j) \end{aligned} \tag{7}$$

where h_0 is a constant and $h_j(.)(j\neq 0)$ is the *jth*-order kernels of the Volterra model.

In practical applications, the full Volterra filter cannot be implemented due to its infinite memory resulting in high computational complexity. Therefore, the higher orders are fallen down and the Third-Order Volterra (TOV) model is widely used which can be written as [38]:

$$\mathrm{Y[n]}= \sum_{i_1=0}^{M-1} h_1[i_1]X[n-i_1] + \sum_{i_1=0}^{M-1}\sum_{i_2=0}^{M-1}\sum_{i_3=0}^{M-1} h_3[i_1 i_2 i_3]X[n-i_1]X[n-i_2]X[n-i_3] \tag{8}$$

where h_0=0, $h_1[i_1]$ and $h_3[i_1 i_2 i_3]$ are the linear and cubic Volterra kernel, respectively and *M* denotes the filter memory length.

Note that even-order kernels are neglected since the even order nonlinearities are absent in optical fiber and only odd-order terms are retained [39].

From Eq. (12), it can be seen that TOV equalizer is a combination of linear FIR filter and nonlinear series of third-order terms.

The Recursive Least Squares (RLS) algorithm is employed to update the coefficients of the adaptive filter. Indeed, these coefficients are chosen so that the error function, which is the difference between the desired signal (i.e. reference signal) and the actual output of the filter, is minimized. The structure of the TOV filter with the memory of two (*M*=2) is illustrated in Fig.6, where ten coefficients are needed.

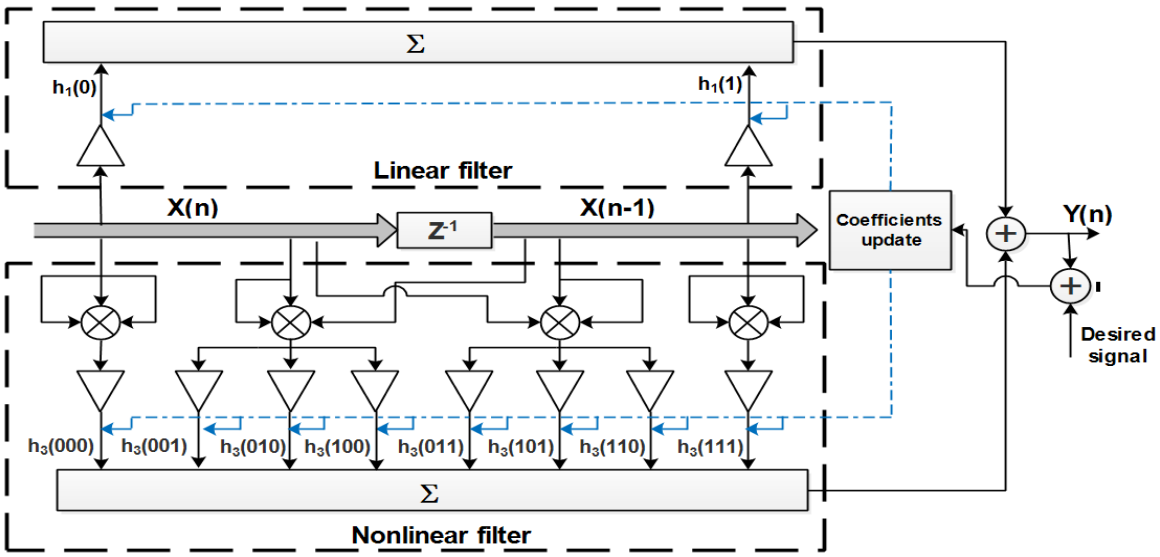

Fig.6. Implementation of third-order Volterra with *M*=2.

4. Results and Discussions

At first glance, we remark that the effects of the Polarization Mode Dispersion (PMD) on the two polarization components are negligible. This can be explained by the fact that the PMD increases with the square root of the transmission distance. In other words, the PMD plays a negligible role for short transmission link.

Fig. 7 shows the Bit Error Rate (BER) as a function of received power for different waveforms using both linear (RLS) and nonlinear (TOV) equalizers.

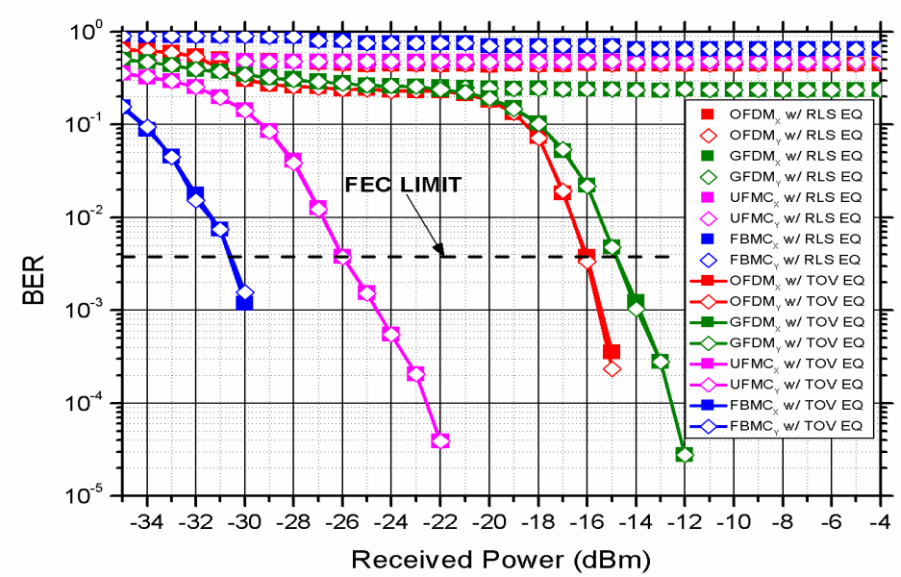

Fig.7. BER vs. received power for different waveforms using RLS (w/o line) and TOV (w/line) filters with 8 taps over 25 Km SMF

As expected, the RLS filter was unable to properly recover the transmitted signal due to the nonlinear effects generated by the interaction between the DFB oscillation output and the chromatic dispersion of the fiber. Whereas, TOV filter with the same number of taps (i.e. 8 taps) shows good performance in terms of BER for all the investigated waveforms. Fig.7 shows that the Forward Error Correction (FEC) limit, which corresponds to input BER ~ 3.810-

[3] [40] for FBMC, UFMC, OFDM and GFDM are obtained at -30.5, -26, -16 and -14.9 dBm, respectively. Compared to traditional OFDM, FBMC-OQAM improves the sensitivity of the receiver by 14.5 dB and 10 dB for UFMC. While GFDM modulation experiences a penalty of 1.1 dB. Indeed, these results can be explained based on two main parameters: *(i)* filtering operation and *(ii)* orthogonality.

As already mentioned, FBMC and GFDM subcarriers are filtered separately, UFMC subcarriers are filtered in groups while OFDM used window filter. In the frequency domain, FBMC has the lowest OOB leakage followed by UFMC, GFDM and then OFDM. Hence, FBMC experiences the smallest Inter-Carrier Interference (ICI), then UFMC and OFDM. It should be noted that for GFDM modulation, despite using per subcarrier filtering, the OOB radiations are slightly higher than UFMC due to the abrupt variations of the signal value between GFDM blocks [41].

According to the first parameter, one may deduce that GFDM modulation reaches the FEC threshold at a received power between UFMC and OFDM modulation which is not the case, in this context, the second parameter comes into play.

For the orthogonality constraint, all the modulation schemes satisfy this condition either in complex or real domain except for GFDM, where the orthogonality between subcarriers is broken. Hence, it undergoes more ICI compared to OFDM.

The constellations diagrams of the 16-QAM dual-polarized signals are plotted in Fig.8. It is interesting to note that the FBMC waveform uses 2x4-PAM constellation (i.e. purely real or imaginary valued), which is equivalent to 16-QAM modulation.

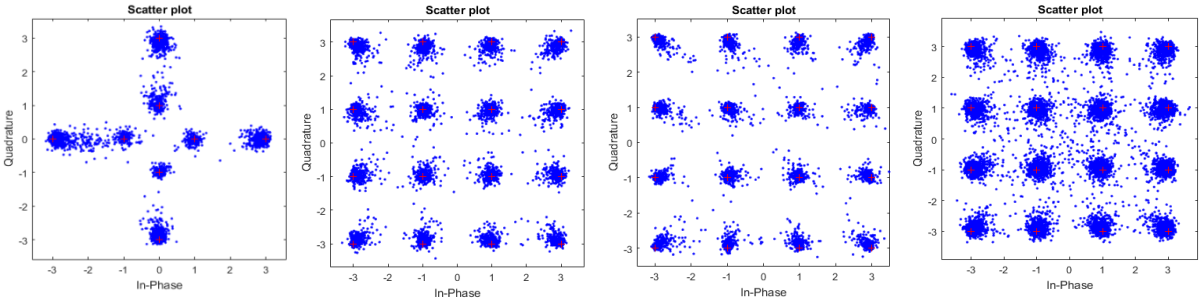

(a) (b) (c) (d)

Fig.8. Constellation diagram for (a) FBMC-OQAM (b) UFMC (c) OFDM (d) GFDM at respectively -30.5,-26, -16 and -14.9 dBm

The impact of deploying DFB laser in our system is investigated and compared to an ideal intensity modulator (without DFB) where the launched optical power is given by the square root of the total electrical current applied to the DFB laser. The *Q* factor parameter, used to measure the transmission link quality, is related to BER by [42]:

$$Q(dB) = 20 \times \log_{10}(\sqrt{2} \times ercf^{-1}(2 \times BER)) \quad (9)$$

where *ercf(.)* is the complementary error function.

As can be seen in Fig.9, the FBMC-OQAM signal is perfectly recovered at a received optical power of -30.5 dBm when an ideal modulator is employed. Indeed, to combat interference, FBMC modulation uses various techniques such as O-QAM modulation, long symbol duration and filtering process is performed for each subcarrier separately. The highest *Q* penalty (Q_{ref} ~ 8.53 dB) of 4.14 dB occurs at -14.9 dBm for GFDM signals. The interplay between laser chirp and fiber dispersion degrades the signal quality in addition to the interference generated by the loss of orthogonality. UFMC and OFDM modulations have almost the same penalties in terms of *Q* factor, which are respectively 2.44 and 2.77 dB when TOV equalizer with 8 taps is used.

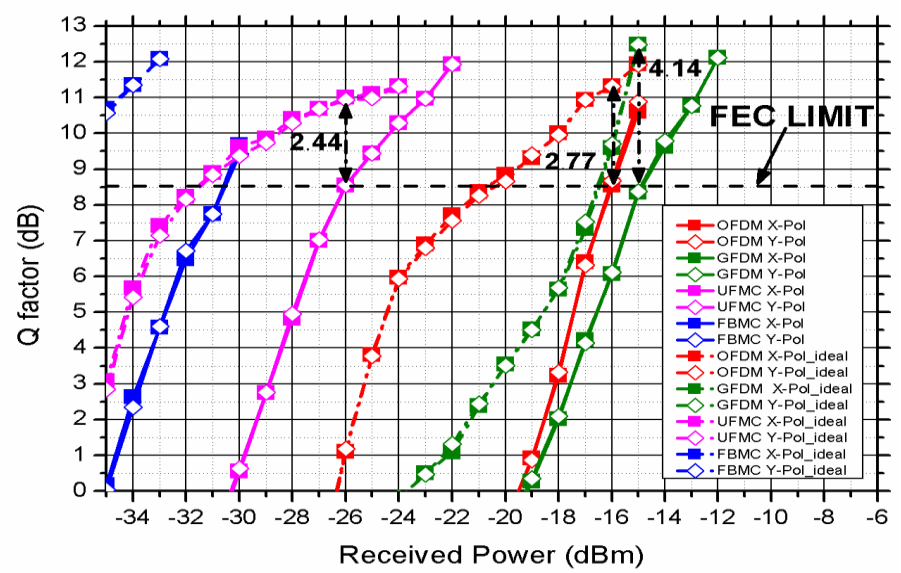

Fig.9. *Q* factor versus received power for different waveforms, including (solid line) and excluding (dashed line) DFB laser.

The investigated waveforms are evaluated by measuring their Error Vector Magnitude (EVM) for different received optical powers. This performance indicator quantifies the difference between the reference symbols (i.e. red points in Fig.8) and the measured symbols. Mathematically, EVM can be expressed as follows [43]:

$$EVM\,(\%) = \sqrt{\frac{\frac{1}{M}\sum_{i=1}^{M}\left|S_i^{reference} - S_i^{measured}\right|^2}{\frac{1}{M}\sum_{i=1}^{M}\left|S_i^{reference}\right|^2}} \qquad (10)$$

where *M* denotes the number of symbols in I-Q constellation. Fig.10. illustrates the EVM performance as a function of the received optical power for different waveforms approach. The emitted symbols are accurately detected as the received power increases and the 3GPP EVM limit of 12.5% [44] is achieved at -31.2, -27.1, -16.2 and -15.5 dBm for FBMC-OQAM, UFMC, OFDM and GFDM modulation, respectively. These different values of received optical powers are approximately conformed to the previous results.

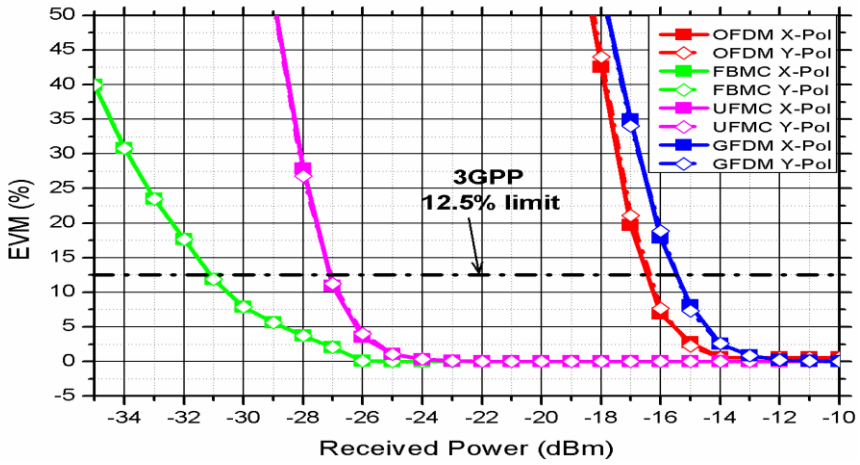

Fig.10 EVM performance versus received optical power for different waveforms

To ensure the feasibility of the implementation depicted in Fig.5, in terms of power budget, the amount of light available between optical source and detector is computed according to the parameters given in table III.

Table III. Power budget parameters

Parameter	Value
Transmitter Power (dBm)	0
Received power (dBm)	-35
Connector loss (dB)	0.5
Splice loss (dB)	0.7
System margin (dB)	6
Fiber loss (dB/Km)	0.2
Amplifier gain (dB)	20

Our implementation requires 14 connectors to connect DFBs, PBC, VOA, EDFA, PS and PDs, resulting a total attenuation of 14×0.5= 7 dB. Splicing process generates 14×0.7= 9.8 dB of attenuation, (1 splice per connector). The total loss of the fiber for the entire path is equal to 5 dB, (0.2×25). Therefore, the total attenuation is equal to 27.8 dB, where the safety margin is taken into account.

Moreover, the required margin is given by the difference between the emitted power and the APD sensitivity, which is equal to 35 dB. Accordingly, a headroom of 33.2 dB is obtained when including the system margin of 6 dB and the EDFA gain.

Therefore, our architecture can be deployed without any performance degradation. Noting that the insertion loss of the PBC and the PS are neglected due to their low contributions.

5. Computational complexity

In this section, we compare all the investigated waveforms in terms of computational complexity at the transmitter side.

The number of real multiplications of OFDM transmitter based on *M*-point FFT using a split-radix algorithm is given by:

$$\begin{aligned} C_{OFDM}^{Tx} &= C_{FFT} \\ &= M \times \left(\log_2(M) - 3\right) + 4 \end{aligned} \tag{11}$$

As shown in Fig.2, FBMC transmitter scheme involves three main blocks, namely, O-QAM pre-processing, IFFT and PPN. For O-QAM pre-processing, just a simple multiplication by a power of *j* (i.e. to maintain orthogonality between subcarriers), so it can be considered as multiplication free. The complexity of the second block (i.e. IFFT) is given in Eq. (15). The resulting signals after the IFFT process are filtered in the time domain with a polyphase filter where the number of multiplications, C_1, depends on the IFFT size (i.e. *M*), and the overlapping factor *K*.

The filter bank is deducted from the prototype filter by performing the frequency shift where the numerical complexity is given in C_2. Assuming that multiplication with the phase rotation is negligible, the resulting complexity of FBMC-OQAM with PPN can be expressed as:

$$\begin{aligned} C_{FBMC-OQAM+PPN}^{TX} &= 2 \times (M \times (\log_2(M) - 3) + 4 + C_1 + C_2) \\ &= 2 \times (M \times (\log_2(M) - 3) + 4 + 2MK + 2M_{active}) \end{aligned} \tag{12}$$

According to Fig.3, the UFMC transmitter has two main steps, namely, IFFT and filtering operation. For each sub-band, linear convolution is performed between IFFT outputs and the filter impulse response. Hence, the complexity implementation of the UFMC transmitter is obtained by summed up all the *B* sub-bands and given by:

$$C_{UFMC}^{TX} = B \times (C_{FFT}(\frac{M}{B}) + 6L(\frac{M}{B}) + 2(L-1)(\frac{M}{B}-1)) \qquad (13)$$

In Eq. (17), *L* denotes the filter length.

For GFDM, the output signal can be mathematically expressed as a multiplication between modulation matrix, *A*, of size *KM* × *KM* and the symbols vector of size *KM* × *1*. In this way, the number of complex multiplications can be calculated as:

$$C_{GFDM}^{TX} = (K \times M)^2 \qquad (14)$$

According to Eq. (16), (17), (18), the computational complexity of FBMC-OQAM with PPN, UFMC and GFDM is much higher than OFDM. Indeed, the FBMC-OQAM approach increases with the overlapping factor *K*, whereas UFMC complexity is proportional to the number of sub-band. In [45], the authors summarized the computational complexity of the proposed 5G and beyond waveforms where the UFMC approach has the highest complexity due to increased FFT size at the receiver followed by GFDM, FBMC and then OFDM.

6. Conclusion

In our paper, we assess for the first time the performance of 25 Gbps dual-polarized 5G waveforms and beyond in directly modulated DFB-laser over 25 Km of single-mode fiber using Volterra equalizer. Our simulation results show that FBMC-OQAM with PPN structure is the most resilient to subcarrier-to-subcarrier intermixing interferences with acceptable complexity. Adaptive Volterra equalizer is a prominent tool to deal with nonlinear impairments and it is able to show higher performance when increasing the memory depth. However, this enhancement comes at the cost of a more complex burden. Sparse-Volterra filter can be deferred for future works to reduce the arithmetic computations.

7. Acknowledgment

The work of Mr.Sofien Mhatli is under the national project “Programme jeune chercheur”.

References

[1] Recommendation ITU-R M.2083-0, "*IMT Vision – Framework and overall objectives of the future development of IMT for 2020 and Beyond*", Sept. 2015.

[2] ITU-T, SG 13, " Towards a New Internet for the Year 2030 and Beyond"

[3] Ericsson, "*Mobile technology trends: traffic by application category*".

[4] S. J. Nawaz, S. K. Sharma, S.Wyne, M. N. Patwary, MD. Asaduzzaman, " Quantum Machine Learning for 6G Communication Networks: State-of-the-Art and Vision for the Future, IEEE Access, Vol 7, 2019"

[5] C. Lin. I, G. Yu, S. HAN, G.Y. LI, "*Green and Software-defined Wireless Networks From Theory to Practice*", Cambridge University Press,p.182-183, Apr. 2019

[6] K.Mallick, R. Mukherjee, B.Das, G.C.Mandal,A. S. Patra, " Bidirectional hybrid OFDM based Wireless-over-fiber transport system using reflective semiconductor amplifier and polarization multiplexing technique". Int. J. Electron. Common. (AEU) Vol 96, pp 260-266, Nov 2018,

[7] M. Schellmann, Z. Zhao, H. Lin, P. Siohan, N. Rajatheva, V. Luecken, A. Ishaque, "*FBMC-based air interface for 5G mobile: Challenges and proposed solutions*", in IEEE, 9th International Conference on Cognitive Radio Oriented Wireless Networks and Communications (CROWNCOM), Jun. 2014.

[8] T. Wild, F. Schaich, and Y. Chen, "*5G air interface design based on universal filtered (UF-) OFDM*", in Proc. 19th Int. Conf. Digit. Signal, pp. 699–704, Aug. 2014.

[9] G. Fettweis, M. Krondorf and S. Bittner, "*GFDM-Generalized Frequency Division Multiplexing*", in VTC Spring - IEEE 69th Vehicular Technology Conference, Apr. 2009.

[10] R.S. Alhumaima, R.K. Ahmed; H. S. Al-Raweshidy, "*Maximizing the Energy Efficiency of Virtualized C-RAN via Optimizing the Number of Virtual Machines*", IEEE Transactions on Green Communications and Networking, Dec. 2018

[11] A.Abraham P.Krömer V.Snášel, " Advances in Intelligent Systems and Computing ", Springer, Afro-European Conference for Industrial Advancement, Vol 334, 2014

[12] H. Xin, H. He, K. Zhang, S. B.Hussain, W. Hu, "*Flexible Baseband-Unit Aggregation Enabled by Reconfigurable Multi-IF Over WDM Fronthaul*", IEEE Photonics Journal, Feb. 2018

[13] A. Pizzinat, P. Chanclou, F. Saliou, T. Diallo, "*Things You Should Know About Fronthaul*", Journal of Lightwave Technology, Jan. 2015

[14] W. Shieh and I. Djordjevic, "*OFDM for Optical Communications*", New York, NY, USA: Academic, 2009.

[15] S. Sarmiento, A. Gran, J. Altabas, M. Scalabroni, S. Spadaro, I. Garces, J. Lazaro, "*Experimental Assessment of 5-10Gbps 5G Multicarrier Waveforms with Intensity-Modulation Direct-Detection for PONs*", in IEEE Photonics in Switching and Computing (PSC), Cyprus, Sept. 2018.

[16] M. Kasmi, S. Mhatli, F. Bahloul, I. Dayoub, K. Oh, "*Performance analysis of UFMC waveform in graded-index fiber for 5G communications and Beyond*", Optics Communications, Vol.454, Jan. 2020.

[17] J. J. Yu, Z. S. Jia, M. F. Huang, M. Haris, P. N. Ji, T. Wang, and G. K. Chang, "*Applications of 40-Gb/s chirp managed laser in access and metro networks*", journal of Lightwave Technology, Vol. 27, Feb. 2009.

[18] B. L. Espe, "*Matlab simulation of a Distributed FeedBack (DFB) laser with chirp effects",* master thesis, at Naval Postgraduate School, Austin, Dec. 1994

[19] M. Maqusi, "*Performance of baseband digital data transmission on nonlinear channels with memory* ", IEEE Trans. Commun., vol. COM-33, no. 7, pp. 715–719, Jul. 1985.

[20] B. Saltzberg, "*Performance of an Efficient Parallel Data Transmission System*", in IEEE Transactions on Communication Technology, Vol.15, Dec. 1967.

[21] M.G. Bellanger, "*Specification and design of a prototype filter for filter bank based multicarrier transmission*", in IEEE International Conference on Acoustics, Speech, and Signal Processing, vol. 4, pp. 2417–2420, 2001.

[22] A.Viholainen, T. Ihalainen, T. Stitz, M. Renfors, and M. Bellanger, "*Prototype filter design for filter bank based multicarrier transmission*", in 17th European Signal Processing Conference (EUSIPCO 2009) Glasgow, Scotland, Aug. 2009.

[23] M. Bellanger, D. Le Ruyet, D. Roviras, M. Terré, J. Nossek, L. Baltar, Q. Bai, D. Waldhauser, M. Renfors, T. Ihalainen et al. "*FBMC Physical Layer: A Primer*". PHYDYAS, 2010.

[24] PHYDYAS – PHYsical layer for DYnamic AccesS and cognitive radio, "*Prototype filter and structure optimization*", D5.1, Jan.2009

[25] M. Shaat and F. Bader, "*Low complexity power loading scheme in cognitive radio networks: FBMC capability*", in IEEE, 20th International Symposium on Personal, Indoor and Mobile Radio Communications, 2009.

[26] G.C.Mandal, R.Mukherjee, K.Mallick, P.Mandal, and A.S.Patra " Bidirectional carrier aggregation in next-generation radio-over-fiber heterogeneous network based on FBMC ", Chinese Optics Letters Vol. 17,Iss 6, pp. 060602-, 2019

[27] F. Schaich, T. Wild, and Y. Chen, "*Waveform contenders for 5G suitability for short packet and low latency transmissions*", in Proc. IEEE 79th Veh. Technol. Conf. (VTC Spring), pp. 1–5, May 2014.

[28] L.D. Paarmann, "*Design and analysis of analog filters A Signal Processing Perspective*", The International Series in Engineering and Computer Science book series, pp.132
[29] B.M. Alves, L.L. Mendes, D.A. Guimaraes, and I.S. Gaspar, "*Performance of GFDM over frequency-selective channels*", in Proc. Int. Workshop Telecommun., 2013.
[30] N. Michailow, M. Matthé, I. Gaspar, A.N.Caldevilla, L.L.Mendes, A.Festag, G. Fettweis, "*Generalized Frequency Division Multiplexing for 5th Generation Cellular Networks*", IEEE Transactions on Communications, Sept. 2014
[31] R. Datta, N. Michailow, M. Lentmaier and G. Fettweis, "*GFDM Interference Cancellation for Flexible Cognitive Radio PHY Design*", in 2012 IEEE Vehicular Technology Conference (VTC Fall), Sept. 2012.
[32] M.Matthé, N.Michailow, I.Gaspar, G. Fettweis, "*Influence of pulse shaping on bit error rate performance and out of band radiation of Generalized Frequency Division Multiplexing*" IEEE International Conference on Communications Workshops (ICC), 2014
[33] F. Da Ros, S. Civelli, S. Gaiarin, E.P. da Silva, N. De Renzis, M. Secondini, and D. Zibar," Dual-polarization NFDM transmission with continuous and discrete spectral modulation", IEEE Journal of Lightwave Technology, 2018
[34] G. Baskara, M. Suryanegara, "*Study of Filter-Bank Multi Carrier (FBMC) Utilizing Mirabbasi-Martin Filter for 5G System*", IEEE, 15th International Conference on Quality in Research (QiR): International Symposium on Electrical and Computer Engineering, Jul. 2017
[35] S. Hu, X. Yi, J. Zhang, Y. Song, M. Zhu, K. Qiu, "*Volterra equalization of complex modulation utilizing frequency chirp in directly modulated lasers*", Optics Communications Vol. 409, p. 99-104 Feb. 2018
[36] N. André, K. Habel, H. Louchet, A. Richter, "*Equalization Techniques for High-Speed OFDM-Based Access Systems Using Direct Modulation and Direct Detection*", IEEE, ICTON 2013
[37] J.Pan, Chi-H.Cheng," Nonlinear Electrical Compensation for the Coherent Optical OFDM System ", IEEE Journal of Lightwave Technology, Vol. 29, No. 2, Jan 15, 2011
[38] S. Im, "*Adaptive equalization of nonlinear digital satellite channels using a frequency-domain Volterra filter*", Proceeding of MILCOMS. IEEE Military Communications Conference
[39] K.V. Peddanarappagari ,M.B.Pearce, *"Volterra Series Transfer Function of Single-Mode Fibers"* Journal of Lightwave Technology, Vol. 15, No. 12, DEC 1997.
[40] R.-J. Essiambre, G. Kramer, P. J. Winzer, G. J. Foschini, B.Goebel, "*Capacity Limits of Optical Fiber Networks*", Journal of Lightwave Technology, Feb. 2010.
[41] H.K. Bizaki, "*Towards 5G Wireless Networks: A Physical Layer Perspective*", Dec 2016
[42] W. Freude, R. Schmogrow, B. Nebendahl, M. Winter, A. Josten, D. Hillerkuss, S. Koenig, J. Meyer, M. Dreschmann, M.Huebner, C. Koos, J. Becker, J. Leuthold, "*Quality metrics for optical signals: eye diagram, Q factor, OSNr, EVM and BER*", International Conference on Transparent Optical Networks (ICTON), 2012
[43] S. Forestier, P. Bouysse, R. Quere, A. Mallet, J.M. Nebus, L. Lapierre, "*Joint Optimization of the Power-Added Efficiency and the Error-Vector Measurement of 20-GHz pHEMT Amplifier Through a New Dynamic Bias-Control Method*", IEEE Transactions on Microwave Theory and Techniques, Apr. 2004
[44] ETSI, "*LTE; Evolved universal terrestrial radio access (E-UTRA); Base station (BS) radio transmission and reception*", 2015.
[45] A. Hammoodi, L. Audah, M.A. Taher, "*Green Coexistence for 5G Waveform Candidates: A Review*", IEEE Access, Jan. 2019